THE JOURNAL OF BIOLOGICAL CHEMISTRY VOL. 286, NO. 4, pp. 2607–2616, January 28, 2011

Autophosphorylation Activates *Dictyostelium* Myosin II Heavy Chain Kinase A by Providing a Ligand for an Allosteric Binding Site in the α-Kinase Domain*[S]

Received for publication, August 19, 2010, and in revised form, October 24, 2010 Published, JBC Papers in Press, November 11, 2010, DOI 10.1074/jbc.M110.177014

Scott W. Crawley[‡], Mojdeh Samimi Gharaei[‡], Qilu Ye[‡], Yidai Yang[‡], Barak Raveh[§], Nir London[§], Ora Schueler-Furman[§], Zongchao Jia[‡1], and Graham P. Côté[‡2]

From the [‡]Department of Biochemistry, Queen's University, Kingston, Ontario K7L 3N6, Canada and the [§]Department of Microbiology and Molecular Genetics, Institute for Medical Research Israel-Canada, Hadassah Medical School, The Hebrew University, Jerusalem, 91120 Israel

Dictyostelium discoideum **myosin II heavy chain kinase A (MHCK A), a member of the atypical α-kinase family, phosphorylates sites in the myosin II tail that block filament assembly. Here we show that the catalytic activity of A-CAT, the α-kinase domain of MHCK A (residues 552–841), is severely inhibited by the removal of a disordered C-terminal tail sequence (C-tail; residues 806–841). The key residue in the C-tail was identified as Thr^{825}, which was found to be constitutively autophosphorylated. Dephosphorylation of Thr^{825} using shrimp alkaline phosphatase decreased A-CAT activity. The activity of a truncated A-CAT lacking Thr^{825} could be rescued by P_i, phosphothreonine, and a phosphorylated peptide, but not by threonine, glutamic acid, aspartic acid, or an unphosphorylated peptide. These results focused attention on a P_i-binding pocket located in the C-terminal lobe of A-CAT. Mutational analysis demonstrated that the P_i-pocket was essential for A-CAT activity. Based on these results, it is proposed that autophosphorylation of Thr^{825} activates ACAT by providing a covalently tethered ligand for the P_i-pocket.** ***Ab initio*** **modeling studies using the Rosetta FloppyTail and FlexPepDock protocols showed that it is feasible for the phosphorylated Thr^{825} to dock intramolecularly into the P_i-pocket. Allosteric activation is predicted to involve a conformational change in Arg^{734}, which bridges the bound P_i to Asp^{762} in a key active site loop. Sequence alignments indicate that a comparable regulatory mechanism is likely to be conserved in** ***Dictyostelium*** **MHCK B-D and metazoan eukaryotic elongation factor-2 kinases.**

Dictyostelium discoideum MHCK A[3] is a highly specialized protein kinase that targets three threonine residues located in the α-helical coiled-coil tail of myosin II (1–4). Phosphorylation of these sites results in the disassembly of myosin II bipolar filaments and inhibits processes, such as cytokinesis, that depend on myosin II contractile activity (5, 6). MHCK A is 130-kDa in size and consists of an N-terminal α-helical coiled-coil domain, a central kinase domain, and a C-terminal WD-repeat domain (7). The coiled-coil domain assembles into trimers or tetramers, binds, and cross-links actin filaments and is responsible for targeting MHCK A to actin-rich cellular protrusions (8–10). The WD-repeat domain interacts with filamentous myosin II and is required for MHCK A to efficiently phosphorylate myosin II (10, 11). The kinase domain of MHCK A bears no sequence similarity to the superfamily of "conventional" eukaryotic protein kinases but instead belongs to a small but widespread family of atypical protein kinases termed the α-kinases (12).

In addition to MHCK A, *D. discoideum* expresses five proteins with α-kinase domains. Three of the proteins, termed MHCK B, C, and D, are closely related to MHCK A and at least two to them, MHCK B and C, function cooperatively to regulate myosin II filament assembly *in vivo* (13–15). The other two α-kinases, AK1 and VwkA, have domain structures unrelated to MHCK A. AK1 contains an Arf GTPase-activating protein domain and VwkA contains an N-terminal von Willebrand factor A-like domain. The function of AK1 is not known, whereas VwkA is involved in the regulation of contractile vacuole function (16, 17). Mammals express six multidomain proteins with α-kinase domains (12). These include TRPM6 and TRPM7, which function as divalent cation channels and phosphorylate the tail of non-muscle myosin II (18, 19) and eEF2K, which regulates protein synthesis (20).

The isolated α-kinase domain of MHCK A, termed A-CAT, displays a high level of protein kinase activity and strongly prefers to phosphorylate threonine residues (21, 22). The x-ray crystal structure of A-CAT reveals that it is composed of an N-terminal and C-terminal lobe with the active site situated in a cleft at the interface between the two lobes (23). An invariant catalytic residue in the active site (Asp^{766}) can be phosphorylated, suggesting that the α-kinase catalytic mecha-

* This work was supported in part by Canadian Institutes of Health Research Grant MOP8603 and Heart and Stroke Foundation of Ontario Grant T6054 (to G. P. C.), Natural Sciences and Engineering Research Council of Canada Grant 203705 (to Z. J.), the Israel Science Foundation funded by Israel Academy of Science and Humanities ISF Grant 306/6, and USA-Israel Bi-national Science Foundation Grant 2009418 (to O. S.-F.).

[S] The on-line version of this article (available at http://www.jbc.org) contains supplemental Table S1 and Figs. S1–S5.

The atomic coordinates and structure factors (code 3PDT) have been deposited in the Protein Data Bank, Research Collaboratory for Structural Bioinformatics, Rutgers University, New Brunswick, NJ (http://www.rcsb.org/).

[1] Canada Research Chair in Structural Biology.

[2] To whom correspondence should be addressed. Tel.: 613-533-2998; Fax: 613-533-2497; E-mail: coteg@queensu.ca.

[3] The abbreviations used are: MHCK, *D. discoideum* myosin II heavy chain kinase; A-CAT, the α-kinase domain of MHCK A; AK1, *D. discoideum* α-kinase 1; eEF2K, eukaryotic elongation factor-2 kinase; MBP, myelin basic protein; TRPM, transient receptor potential melastatin; P_i, inorganic phosphate; SAP, shrimp alkaline phosphatase; TES, 2-{[2-hydroxy-1,1-bis(hydroxymethyl)ethyl]amino}ethanesulfonic acid.

nism differs from that of conventional eukaryotic protein kinases. A-CAT contains a tightly bound zinc atom that is required for stability and binds two Mg^{2+} ions, one in an active site pocket and one at the center of the glycine-rich N/D-loop. The Mg^{2+} binding sites are regulatory, because millimolar concentrations of Mg^{2+}, in excess of that required to bind to ATP, are required for A-CAT to exhibit maximal catalytic activity (22). A-CAT also binds a P_i molecule at a highly basic site in the C-terminal lobe that we term the P_i-pocket (23).

The catalytic activity of MHCK A is enhanced at least 50-fold by autophosphorylation (24). The cellular signaling mechanisms that activate MHCK A remain to be elucidated, but *in vitro* the rate of autophosphorylation is stimulated by actin filaments, myosin II, and negatively charged compounds, such as DNA and acidic phospholipids (25, 26). MHCK A incorporates up to 10 mol of phosphate/mol, but 3 mol of phosphate are sufficient for maximal activation (24). Here we identify Thr^{825} as a key autophosphorylation site that is required for the activity of A-CAT and MHCK A. Thr^{825} is located within a disordered sequence that links the α-kinase domain to the WD-repeat domain. We further demonstrate that the P_i-pocket functions as a positive allosteric binding site, and propose a model in which the phosphorylated Thr^{825} ($Thr(P)^{825}$) activates A-CAT by providing a covalently tethered ligand for the P_i-pocket. Sequence alignments indicate that the proposed regulatory mechanism is conserved in the other MHCKs and the metazoan eEF2Ks.

EXPERIMENTAL PROCEDURES

Materials—Peptides used in this study were synthesized by the Sheldon Biotechnology Facility, McGill University. ATP, MBP, aspartic acid, glutamic acid, threonine, and phosphothreonine were purchased from Sigma and [γ-^{32}P]ATP was obtained from PerkinElmer Life Sciences.

Plasmid Constructs—DNA manipulations were carried out using standard methods (27). Truncation and deletion constructs of the MHCK A α-kinase domain (A-CAT; residues 552–841) were created using PCR (22). DNA constructs encoding site-directed mutants of A-CAT were generated using the QuikChange XL site-directed mutagenesis system (Stratagene). Constructs were cloned in-frame into the NcoI and XhoI sites of the pET-28a vector (Novagen) to add an N-terminal His tag and a TEV protease site as described (23). Full-length MHCK A constructs (NCBI accession XP_635600) were cloned into the plasmid pTX-FLAG vector (28) that had been adapted to GATEWAY technology (Invitrogen). Briefly, the parent plasmid pTX-FLAG was digested by BamHI and XhoI and blunted with T4 DNA polymerase. The Gateway recombination cassette (reading frame cassette B) was then inserted to create destination vector pTX-FLAG-GATE. Expression constructs encoding MHCK A were then created using pTX-FLAG-GATE according to the manufacturer's instructions.

Protein Expression and Purification—Wild-type and mutant forms of A-CAT were expressed in *Escherichia coli* BL21(DE3) and purified by chromatography over a His-Bind column (Novagen) as described (supplemental Fig. S1) (23, 29). FLAG-tagged MHCK A was expressed in the *D. discoideum* AX3 cell line (30). Cells were cultured on 9-cm plastic Petri dishes in HL5 medium (31) supplemented with 10,000 units/ml of penicillin and 10 mg/ml of streptomycin (Sigma). Plasmids were introduced into AX3 cells by electroporation at 0.85 KV and 25 microfarads using a Bio-Rad Gene Pulser II Electroporation System (32). Clonal cell lines expressing FLAG-tagged MHCK A were produced by dilution plating and selection in 20 μg/ml of geneticin (G418) (Invitrogen). Cells were lysed by homogenization in 500 mM NaCl, 1 mM EDTA, 0.3% Triton X-100, and 50 mM Tris-HCl, pH 8.0, containing one complete mini protease inhibitor tablet (Roche Applied Diagnostics) per 50 ml of buffer at 4 °C. The supernatant obtained following centrifugation at 12,000 $\times$ *g* for 1 h was passed over a column of anti-FLAG M2 Affinity gel (Sigma) (33). FLAG-MHCK A was eluted with TBS buffer (150 mM NaCl, 50 mM Tris-HCl, pH 7.4) containing 200 μg/ml of FLAG peptide and dialyzed against 20 mM NaCl and 50 mM Tris-HCl, pH 7.4.

Kinase, ATPase, and Autophosphorylation Assays—ATPase and kinase activity was assayed at 22 °C in kinase buffer (2 mM $MgCl_2$, 1 mM dithiothreitol, 0.25 mM ATP, and 20 mM TES, pH 7.0) containing [γ-^{32}P]ATP at a specific activity of 5–500 cpm/pmol of ATP. Kinase assays included MBP or the MH-3 synthetic peptide (RKKFGEAEKTKAKEFL) at a concentration of 30 or 300 μM, respectively. Other additions to the kinase and ATPase assays are described in the figure legends. Assays were initiated by the addition of 1.45 μM A-CAT or 38.8 nM MHCK A. Aliquots were removed at 1, 2, 3, 4, and 5 min for kinase assays and 5, 10, 20, and 40 min for ATPase assays. In some cases kinase assays were performed at 4 °C and aliquots were removed at 20, 40, 60, and 90 s. ATP hydrolysis was measured by following the release of ^{32}P (34). Kinase activity was measured by spotting 20-μl aliquots onto squares of Whatman P81 phosphocellulose paper (35). The squares were washed in 1% phosphoric acid, immersed in ScintiVerse Universal LS Mixture (Fisher Scientific), and counted using a Beckman LS 9000 scintillation counter. Over the assay time courses linear rates of ATPase activity and phosphate incorporation were obtained. Under the assay conditions used here A-CAT exhibited an ATPase activity of $0.022 \pm 0.002\ s^{-1}$ and a kinase activity of $0.047 \pm 0.004\ s^{-1}$ and $0.101 \pm 0.0029\ s^{-1}$ toward MBP and MH-3, respectively. MHCK A exhibited a kinase activity of $0.19 \pm 0.033\ s^{-1}$ toward MBP. Autophosphorylation assays contained 14.5 μM A-CAT-5xA and were carried out in kinase buffer containing [γ-^{32}P]ATP at a specific activity of 500 cpm/pmol of ATP. Aliquots of 20 μl were taken at 1, 5, 10, 20, 40, and 60 min and subjected to SDS-PAGE. After staining with Coomassie Blue the A-CAT-5xA band was excised and counted in scintillation fluid to measure incorporation of ^{32}P. For some assays A-CAT-5xA was dephosphorylated by treatment at room temperature for 1 h with 10 units of calf intestinal alkaline phosphatase-agarose beads (Sigma) or for 5 h with 10 units of SAP (Fermentas). A total of 200 μg of A-CAT-RRGT or A-CAT-RRGS were incubated with 0.5 μg of recombinant PKA catalytic subunit (Active Motif) for 30 min at 22 °C in kinase buffer. Following dialysis against 20 mM Tris-HCl, pH 7.4, kinase assays were carried out using the MH-3 peptide as de-

scribed above. Data were fit to a hyperbolic equation by nonlinear regression analysis using the program SigmaPlot (Systat Software Inc.). Where shown, mean ± S.D. are derived from 3 to 6 determinations.

Crystallization Procedures and Data Collection and Analysis—A-CAT truncated at Leu^{809} (A-CAT-Δ809) was concentrated to 230 μM using a 10,000 molecular weight cutoff Ultrafree-4 Centrifugal Filtration Unit (Millipore). The His tag was cleaved off by incubation overnight at 4 °C with AcTEV protease (Invitrogen), and the protease was removed by chromatography over a His-Bind column. A 1-μl aliquot of A-CAT-Δ809 was mixed with 1 μl of reservoir solution consisting of 0.1 M Tris-HCl, pH 8.5, 0.2 M NaH_2PO_4, and 18% (w/v) PEG 8000. Crystallization was performed by the hanging drop vapor diffusion method at 4 °C. Crystals of A-CAT-Δ809 appeared after a few days and grew to their maximum size in 10 days. Crystals were flash frozen in a stream of liquid nitrogen after dipping them in a cryoprotectant solution that consisted of the mother liquor component and 25% (w/v) ethylene glycol. A 1.9-Å dataset for the A-CAT-Δ809 crystal was collected at the F1 beamline at the Cornell High Energy Synchrotron Source (CHESS). The dataset was processed and scaled with DENZO and SCALEPACK or with the HKL2000 suite program (36) and solved by molecular replacement with the initially solved A-CAT structure (23) as the search model with PHASER software (37). CNS and REFMAC5 were used to build and refine the final model (38, 39).

Modeling of the C-tail—Ab initio structure prediction methods were used to generate a three-dimensional model of the C-terminal tail sequence (C-tail) with Thr^{825} at the P_i-pocket or the active site. Residues 806 to 830 were first added in an extended conformation (±135° ϕ/ψ angles) to the crystal structure of A-CAT (Protein Data Bank code 3LLA, chain B). The side chains of the starting model were prepacked using the Rosetta-fixed backbone design/packing application (using the parameters -ex1, -ex2, use_input_sc). A three-stage modeling protocol was then applied. In the first step the FloppyTail protocol was used to generate 5500 structural models of the C-tail using a Rosetta fragment library for 3-mer (40). In the second step, the positions of residues 823–830 from the two top scoring FloppyTail models were refined by applying the FlexPepDock protocol, which accurately models the conformation of peptides that fold upon binding to their receptors (41). In the last step, the Rosetta loop refinement protocol over residues 806–824 was used to connect the FlexPepDock model with the rest of the FloppyTail model (42). To model the C-tail at the P_i-pocket, the protocol was constrained to force the phosphate group of Thr^{825} to create similar hydrogen bonds and salt bridges as the original P_i molecule solved in the crystal structure. To model the C-tail at the active site a soft constraint was imposed in the initial low resolution step that required that the Cβ atom of Thr^{825} be within 3–6 Å of the Cβ atom of Asp^{756}, which is presumed to act as the catalytic base in the phosphotransferase reaction (23). This constraint was removed in the subsequent high-resolution modeling steps of all three stages. An ATP molecule at the active site was included, starting from its orientation in the A-CAT-D766A structure (PDB code 3LMI).

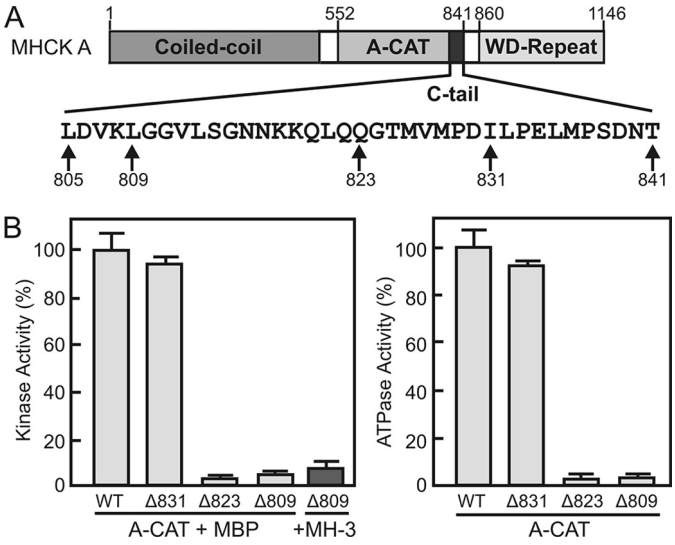

FIGURE 1. **Truncation of the C-tail inhibits the kinase and ATPase activities of A-CAT.** *A*, schematic diagram showing the domain organization of MHCK A. A-CAT encompasses the entire α-kinase domain and part of the unstructured sequence (C-tail) linking the WD-repeat domain. The amino acid sequence of the C-tail is shown with the experimental sites of truncation indicated. *B*, the kinase (*left panel*) and ATPase (*right panel*) activities of wild-type A-CAT (*WT*) and A-CAT truncated at residues 831 (Δ*831*), 823 (Δ*823*), or 809 (Δ*809*) were determined. Removal of residues 823 to 831 from the C-tail resulted in a large decrease in kinase and ATPase activities. Activities were determined from time courses performed as described under "Experimental Procedures" using either MBP or the MH-3 peptide as substrate as indicated. Activities are reported as a percentage of the wild-type activity. *Error bars* represent the standard deviation.

RESULTS

The Disordered C-terminal Sequence Is Required for A-CAT Activity—A-CAT is a catalytically active fragment of MHCK A that encompasses the α-kinase domain (residues 552–805) as well as part of the flexible linker that connects the α-kinase domain to the WD-repeat domain (residues 806–841) (Fig. 1*A*) (22, 23). In the x-ray crystal structure of A-CAT, residues 806–841 lack defined electron density and thus form a disordered C-terminal tail (C-tail) (23). Truncation of the C-tail at residue 831 did not alter the kinase activity of A-CAT, but truncation at residues 823 or 809 resulted in the loss of 90–95% of kinase activity (Fig. 1*B*, *left panel*). The severe loss of kinase activity was observed with both myelin basic protein and the MH-3 peptide, which corresponds to the Thr^{2029} site in the myosin II tail, as substrate (24). In the absence of a protein or peptide substrate A-CAT exhibits a basal rate of ATPase activity (23). Truncation of the C-tail at residues 823 or 809 reduced the ATPase activity of A-CAT by ~95% (Fig. 1*B*, *right panel*). A section of the C-tail between residues 823 and 831 is therefore required for both the kinase and ATPase activities of A-CAT.

An Essential Threonine Residue Is Conserved in the C-tail—A multiple sequence alignment of the C-tail regions of *D. discoideum* MHCK A-D and AK1 reveals a conserved Gly-Thr-hydrophobic motif (Fig. 2*A*). In A-CAT the conserved threonine residue is Thr^{825}, which lies within the region defined by truncation analysis (residues 823–831) as being critical for A-CAT activity. Thr^{825} has been identified by mass spectrometry as one of six autophosphorylation sites in A-CAT (23). The other five autophosphorylation sites (Ser^{553}, Thr^{612},

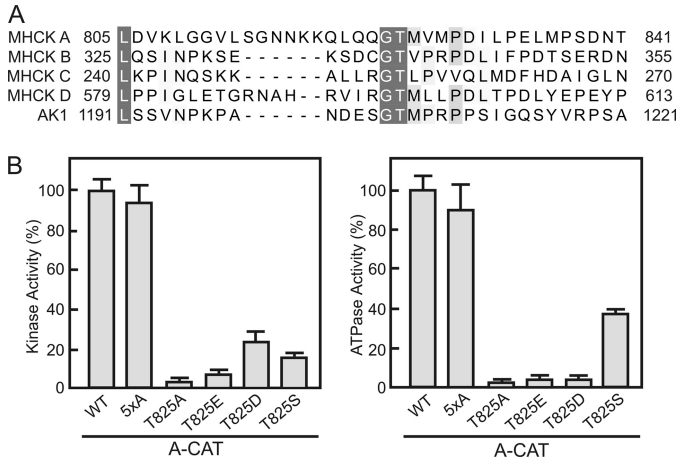

FIGURE 2. **The conserved Thr^{825} residue in the C-tail is required for A-CAT activity.** *A*, a multiple sequence alignment of the C-tail regions of *D. discoideum* MHCK A, MHCK B, MHCK C, MHCK D, and AK1. Conserved residues are shaded in *gray*. A Gly-Thr motif (residues 824 and 825 in MHCK A) is present in all of the C-tail sequences. The NCBI accession numbers are: MHCK A, XP_635119; MHCK B, XP_636368; MHCK C, XP_635600; MHCK D, XP_640080; and AK1, XP_629868. *B*, the kinase (*left panel*) and ATPase (*right panel*) activities of wild-type A-CAT (*WT*), A-CAT-5xA, and the indicated Thr^{825} mutants were determined. Mutation of Thr^{825} severely inhibited both the kinase and ATPase activities of A-CAT. Activities were determined from time courses performed as described under "Experimental Procedures" and the activities are reported as a percentage of A-CAT activity. *Error bars* represent the standard deviation.

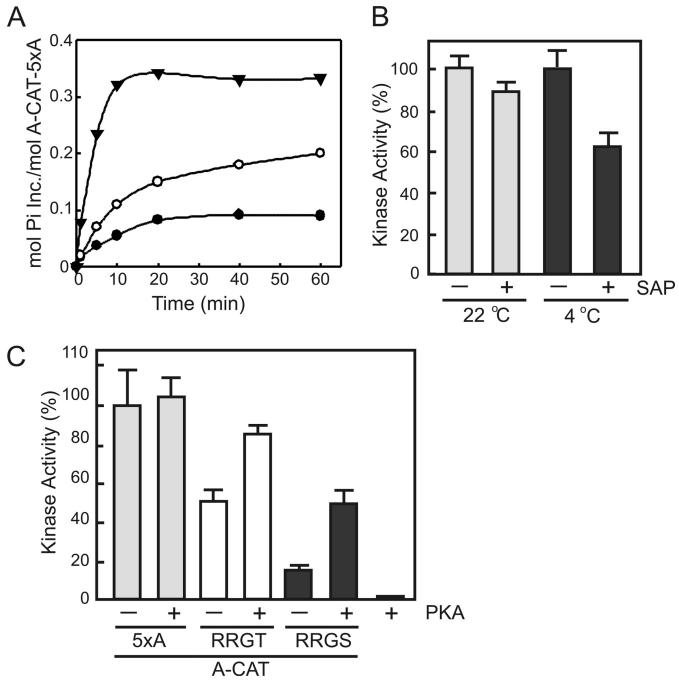

FIGURE 3. **Phosphorylation of the C-tail activates A-CAT.** *A*, time course of the autophosphorylation of A-CAT-5xA prior to treatment (●) and following treatment for 1 h with calf intestinal alkaline phosphatase (○) or for 5 h with SAP (▼). The low level of ^{32}P incorporation indicates that Thr^{825} is highly phosphorylated and is resistant to dephosphorylation by calf intestinal alkaline phosphatase and SAP. Autophosphorylation assays were performed by incubating A-CAT-5xA with [γ-^{32}P]ATP as described under "Experimental Procedures." *B*, the kinase activity of A-CAT-5xA incubated for 5 h in the presence or absence of SAP was assayed at 22 and 4 °C. The assays at 4 °C, which limits the ability of A-CAT-5xA to autophosphorylate Thr^{825}, showed that dephosphorylation of Thr^{825} by SAP decreased the kinase activity of A-CAT-5xA. Activities were determined from time courses performed as described under "Experimental Procedures" and are reported as a percentage of the untreated A-CAT-5xA activity. *Error bars* represent the standard deviation. *C*, the kinase activities of A-CAT-5xA (*5xA*) or A-CAT-5xA with the QQGT sequence in the C-tail mutated to RRGT or RRGS were determined before and after incubation with PKA as indicated. Activities were determined from time courses performed as described under "Experimental Procedures" with the MH-3 peptide as substrate. The MH-3 peptide was not a substrate for PKA. Incubation with PKA activated the RRGT and RRGS mutants, but not A-CAT-5xA, showing that phosphorylation of the Thr^{825} site enhances kinase activity. Activities are reported as a percentage of A-CAT-5xA activity. *Error bars* represent the standard deviation.

Thr^{613}, Thr^{614}, and Thr^{634}) are located within the N-terminal lobe. Mutation of Ser^{553}, Thr^{612}, Thr^{613}, Thr^{614}, and Thr^{634} to alanine (A-CAT-5xA) had little effect on the kinase or ATPase activities of A-CAT (Fig. 2*B*). In contrast, mutation of Thr^{825} to alanine decreased kinase and ATPase activities by 95% (Fig. 2*B*). This result suggests that autophosphorylation of Thr^{825} is critical for the activity of A-CAT. Mutation of Thr^{825} to glutamic acid or aspartic acid resulted in the loss of ~90 and 75% of kinase activity, respectively, indicating that a negatively charged residue only weakly compensates for the loss of phosphothreonine (Fig. 2*B*). A mutant with serine in place of Thr^{825} also exhibited low kinase and ATPase activity (Fig. 2*B*). Serine residues are poor substrates for A-CAT, suggesting that the low activity may reflect the incomplete autophosphorylation of Ser^{825} (21, 29).

Phosphorylation of the C-tail Activates A-CAT—Incubation of A-CAT-5xA with [γ-^{32}P]ATP resulted in the incorporation of less than 0.1 mol of phosphate/mol (Fig. 3*A*). The amount of phosphate incorporated into A-CAT-5xA increased to 0.2 mol/mol after a 1-h treatment with calf intestinal alkaline phosphatase and to 0.33 mol/mol after a 5-h treatment with SAP (Fig. 3*A*). We interpret these results to indicate that Thr^{825} is nearly fully phosphorylated in bacterially expressed A-CAT-5xA and that it is only partially dephosphorylated even after extensive phosphatase treatment. The phosphorylated state of Thr^{825} was confirmed by mass spectrometry (data not shown). Kinase assays showed that SAP treatment produced only a small decrease in the kinase activity of A-CAT-5xA (Fig. 3*B*). It was reasoned that this may reflect the ability of A-CAT-5xA to rapidly autophosphorylate Thr^{825} in the kinase assay (Fig. 3*A*). When kinase assays were carried out at 4 °C to reduce the rate of Thr^{825} autophosphorylation, a significant decrease in the activity of SAP-treated A-CAT-5xA could be detected (Fig. 3*B*). These results are consistent with the conclusion that phosphorylation of Thr^{825} is required for A-CAT activity.

The ability of Thr^{825} phosphorylation to activate A-CAT-5xA was further examined by mutating Gln^{822} and Gln^{823} to arginine to convert Thr^{825} into a PKA phosphorylation site (*i.e.* QQGT to RRGT). A mutant with serine in place of Thr^{825} (RRGS) was also created. A-CAT-RRGS exhibited a lower initial activity than A-CAT-RRGT, which is consistent with serine being a poorer autophosphorylation site than threonine. Incubation with PKA and MgATP increased the activity of A-CAT-RRGT by 60% and A-CAT-RRGS by more than 3-fold (Fig. 3*C*). The increase in activity was accompanied by the incorporation of 0.25 mol of P_i/mol into A-CAT-RRGS by PKA. Control experiments showed that the activity of A-CAT-5xA was not altered by incubation with PKA and that the MH-3 peptide was not a substrate for PKA (Fig. 3*C*). This

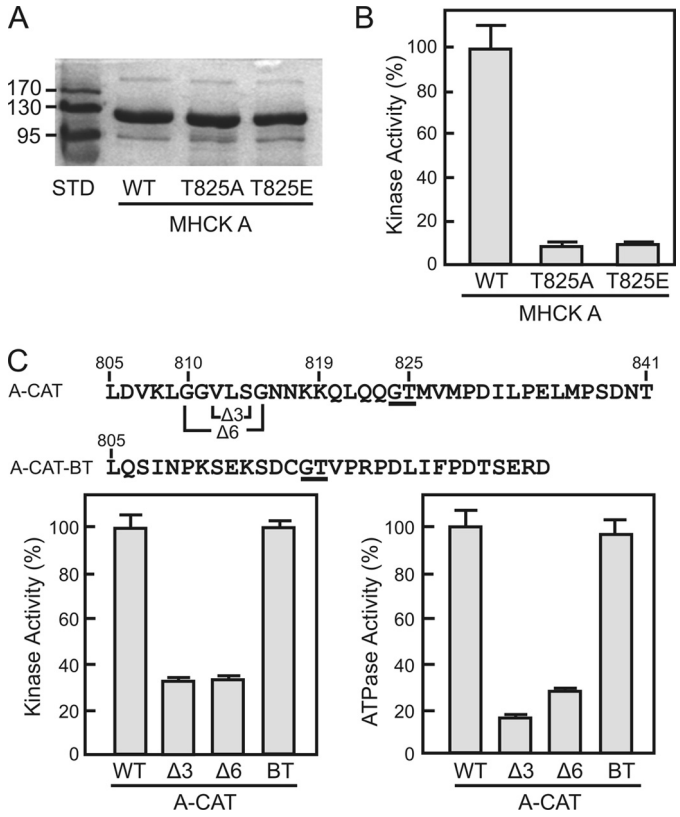

FIGURE 4. **Regulation of A-CAT and MHCK A by Thr825.** *A*, the Coomassie Blue-stained SDS gel shows wild-type MHCK A (*WT*) and the MHCK A T825A and T825E mutants purified from *D. discoideum* as described under "Experimental Procedures." *B*, the kinase activities of MHCK A (*WT*) and the MHCK A T825A and T825E mutants were assayed as described under "Experimental Procedures." Mutation of Thr^{825} severely inhibited the kinase activity of MHCK A. Activities are reported as a percentage of MHCK A activity. *Error bars* represent the standard deviation. *C*, the *top line* shows the sequence of the A-CAT C-tail and indicates the residues deleted to generate the Δ3 and Δ6 constructs. The *second line* shows the sequence of the MHCK B C-tail (residues 326–354) that was fused to Leu^{805} of A-CAT to generate the A-CAT-BT chimera. The conserved Gly-Thr sequence is *underlined*. The kinase (*left panel*) and ATPase (*right panel*) activities of wild-type A-CAT (*WT*), the Δ3 and Δ6 constructs, and the A-CAT-BT chimera (*BT*) were determined from time courses performed as described under "Experimental Procedures." The C-tail of MHCK B rescues the activity of the truncated A-CAT. Activities are reported as a percentage of wild-type A-CAT activity. *Error bars* represent the standard deviation.

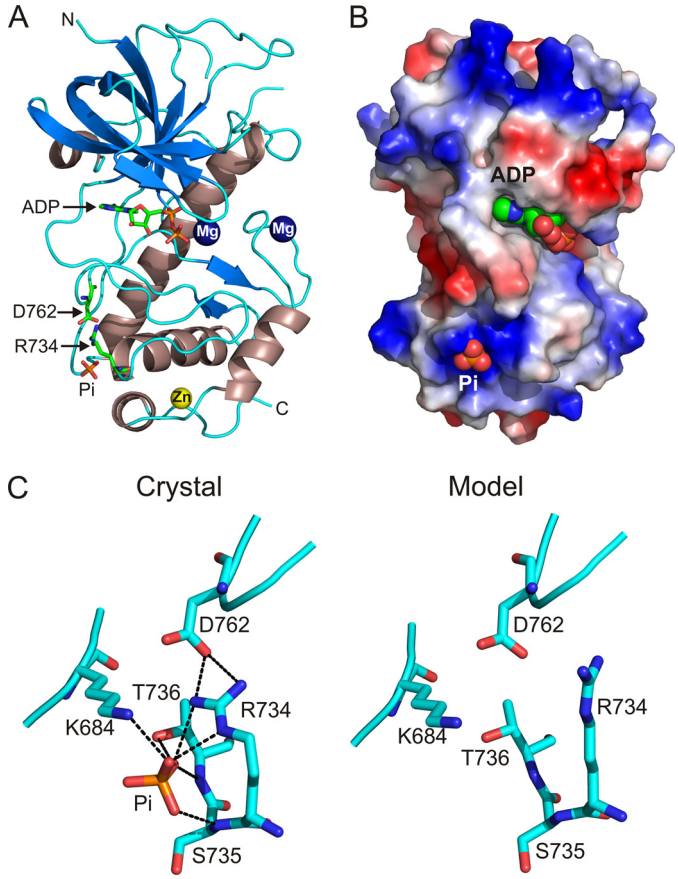

FIGURE 5. **X-ray crystal structure of A-CAT-Δ809.** *A*, the structure of A-CAT-Δ809 is shown with β-strands in *blue* and α-helices in *strawberry*. Mg^{2+} ions are rendered as *dark blue spheres* and the zinc atom as a *yellow sphere*. Arg^{734}, Asp^{762}, ADP, and P_i are shown as *sticks* with the C, O, N, and P atoms colored *green*, *red*, *blue,* and *orange*, respectively. *N*, N terminus; *C*, C terminus. *B*, the distribution of electrostatic potential is shown on the molecular surface of A-CAT-Δ809, with *blue* indicating areas of net positive charge and *red* areas of net negative charge. ADP and P_i are rendered as *spheres*. The view is rotated 40° to the right from the view in *panel A*. *C*, detailed view of the P_i-pocket. The crystal structure of A-CAT (*left panel*) shows that the P_i molecule interacts with the side chains of Arg^{734}, Lys^{684}, and Thr^{736} and the main chain carbonyl of Ser^{735} (*dotted lines*). The bent Arg^{734} side chain bridges the P_i molecule to Asp^{762} in an active site loop. *Ab initio* modeling of the P_i-pocket in the absence of P_i (*right panel*) shows that the side chain of Arg^{734} can switch from the bent to a straight configuration that does not interact with Asp^{762}. Although the straight conformation of Arg^{734} can occur when modeling in the presence of a ligand, it is favored by an empty P_i-pocket. The conformational change in Arg^{734} is postulated to act as an allosteric switch that controls the activity of A-CAT in response to P_i binding.

result provides additional evidence that A-CAT activity depends on the phosphorylation of the Thr^{825} (or Ser^{825}) site in the C-tail.

To examine whether autophosphorylation of Thr^{825} is required for the activation of full-length MHCK A, wild-type MHCK A and T825A and T825E mutants were expressed in *D. discoideum* as FLAG-tagged proteins (Fig. 4*A*). The kinase activities of the MHCK A T825A and T825E mutants were less than 10% that of wild-type MHCK A (Fig. 4*B*). This shows that autophosphorylation of Thr^{825} is a necessary step in the activation of MHCK A.

The effect of moving Thr^{825} closer to the α-kinase domain was examined by deleting three (A-CAT-Δ3) or six (A-CAT-Δ6) residues from the intervening linker sequence (Fig. 4*C*). A-CAT-Δ3 and A-CAT-Δ6 were considerably less active than A-CAT, indicating that the function of Thr^{825} depends to some extent on its position within the C-tail (Fig. 4*C*). The conserved nature of the Gly-Thr-hydrophobic sequence suggested that the C-tails of AK1 and MHCK B-D may have functions comparable with that of MHCK A (Fig. 2*A*). To test this possibility the C-tail of MHCK B (residues 326–354) was fused to the C terminus of A-CAT truncated at Leu^{805} (Fig. 4*C*). The C-tail of MHCK B fully rescued both the kinase and ATPase activity of the truncated A-CAT (Fig. 4*C*). This result supports the view that the MHCK C-tail regions perform analogous regulatory functions.

X-ray Crystal Structure of A-CAT-Δ809—A-CAT truncated at residue 809 (A-CAT-Δ809) was purified in yields comparable with that of A-CAT, showing that the loss of the C-tail does not compromise the stability of the core α-kinase domain. Indeed, A-CAT-Δ809 formed diffraction quality crystals much more readily than A-CAT, indicating that the C-tail

impairs crystal formation. The x-ray crystal structure of A-CAT-Δ809 was solved to a resolution of 1.8 Å (Fig. 5*A* and supplemental Table S1). When the Cα atoms of A-CAT-Δ809 and A-CAT were superimposed, a root mean square difference of 0.37 Å was obtained, which indicates that the two structures are virtually identical. The structure of A-CAT-Δ809 further shows that the absence of the C-tail did not alter the binding of ligands. A-CAT-Δ809, like A-CAT, contained a zinc atom bound to the C-terminal lobe, a P_i molecule bound to the P_i-pocket and Mg^{2+} ions bound at the active site and at the center of the N/D-loop (23). The active site of A-CAT-Δ809 contained ADP, even though crystallization was carried out in a buffer containing ATP (Fig. 5*A*). This result is surprising given the low ATPase activity exhibited by A-CAT-Δ809 (Fig. 1*B*) and raises the possibility that the crystallization conditions induce A-CAT-Δ809 to adopt a catalytically active conformation.

The P_i-pocket Regulates A-CAT Activity—It was reasoned that $Thr(P)^{825}$ must bind to a site in the core α-kinase domain to stimulate catalytic activity. The P_i-pocket, which is located near to the bottom of the C-terminal lobe, provides an obvious candidate for a phosphate-dependent binding site (Fig. 5*B*). The P_i molecule makes electrostatic interactions with the side chains of Lys^{684}, located in the loop following α-helix C, and Arg^{734}, located at the start of α-helix D. The P_i molecule also forms hydrogen bonds with the main chain carbonyl of Ser^{735} and the main chain carbonyl and side chain hydroxyl group of Thr^{736} (Fig. 5*C* and supplemental Fig. S2). Mutation of Lys^{684}, Arg^{734}, and Thr^{736} to alanine reduced the kinase activity of A-CAT by 90–95% showing that an intact P_i-pocket is essential for activity (Fig. 6*A*). A mechanism by which P_i binding may influence the conformation of the active site is apparent from the structure of A-CAT, which shows that Arg^{734} forms a salt bridge with Asp^{762} in one of the principal catalytic loops (Fig. 5*C*). Mutation of Asp^{762} to alanine drastically reduced catalytic activity, demonstrating that the salt bridge with Arg^{734} is of functional importance (Fig. 6*A*).

The possibility that P_i might be able to compensate for the loss of Thr^{825} by providing a ligand for the P_i-pocket was tested by adding NaH_2PO_4 to the kinase assays. The addition of P_i stimulated the kinase activity of A-CAT-Δ809 by ~4-fold, to a level ~20% that of A-CAT (Fig. 6*B*). Half-maximal activation was achieved at a P_i concentration of 440 ± 150 μM. At higher concentrations of P_i a slight inhibition of A-CAT activity was observed, likely because of the increased ionic strength (1). Phosphothreonine proved to be a better activator than P_i, stimulating the kinase activity of A-CAT-Δ809 to a level approaching 65% that of A-CAT (Fig. 6*C*). Half-maximal activation occurred at a phosphothreonine concentration of 250 ± 80 μM. No activation of A-CAT-Δ809 occurred when threonine was added to the kinase assays (Fig. 6*C*). Glutamic acid and aspartic acid also did not activate (not shown). A peptide with a sequence corresponding to residues 823–830 of the C-tail (QQGTMVMPD) had no effect on the activity of A-CAT-Δ809, whereas the phosphorylated version of the peptide (QQG(p)TMVMPD) was as effective an activator as phosphothreonine (Fig. 6*C*). Half-maximal activation

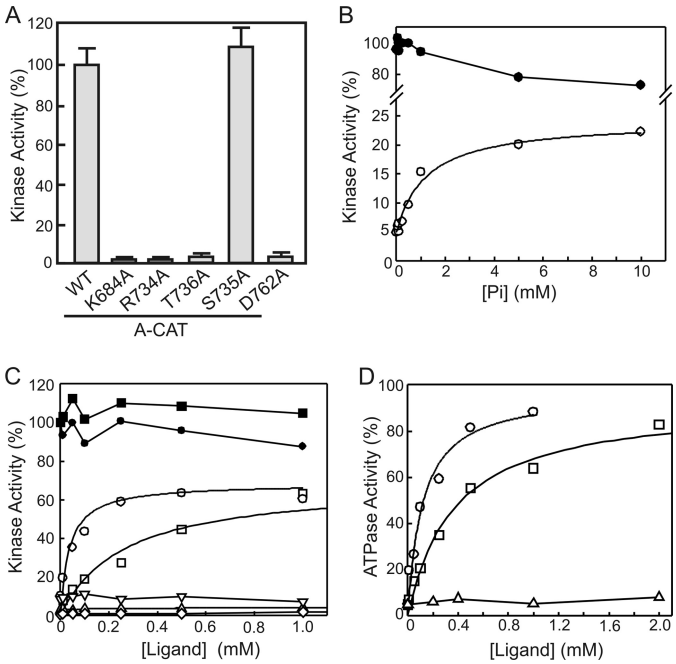

FIGURE 6. **Ligand binding to the P_i-pocket activates A-CAT.** *A*, the kinase activity of wild-type A-CAT (*WT*) and the indicated P_i-pocket mutants were determined as described under "Experimental Procedures." *Error bars* represent the standard deviation. Mutation of residues that bind P_i resulted in a severe loss in kinase activity. *B*, the kinase activity of A-CAT (*closed symbols*) and A-CAT-Δ809 (*open symbols*) were assayed in the presence of NaH_2PO_4. The addition of P_i enhanced the kinase activity of A-CAT-Δ809. A hyperbolic curve fit to the A-CAT-Δ809 data yielded a K_a = 440 ± 150 μM and a V_{max} = 22 ± 3%. Activities are reported as a percentage of the A-CAT activity in the absence of P_i. *C*, the kinase activity of A-CAT (*closed symbols*) and A-CAT-Δ809 (*open symbols*) were assayed in the presence of phosphothreonine (*squares*), the QQG(p)TMVMPD peptide (*circles*), threonine (*triangles*), and the unphosphorylated QQGTMVMPD peptide (*inverted triangles*). The A-CAT-Δ809-R734A mutant was assayed in the presence of phosphothreonine (*diamonds*). Hyperbolic curves fit to the A-CAT-Δ809 data yielded a K_a = 260 ± 80 μM and a V_{max} = 65 ± 6% for phosphothreonine and a K_a = 35 ± 12 μM and a V_{max} = 64 ± 3% for the QQG(p)TMVMPD peptide. Activities are reported as a percentage of the A-CAT activity in the absence of any additions. *D*, the ATPase activity of A-CAT-Δ809 was assayed in the presence of phosphothreonine (*squares*), QQG(p)TMVMPD peptide (*circles*), or threonine (*triangles*). Hyperbolic curves fit to the data yielded a K_a = 360 ± 40 μM and a V_{max} = 93 ± 2% for phosphothreonine and a K_a = 120 ± 40 μM and a V_{max} = 97 ± 8% for the QQG(p)TMVMPD peptide. The kinase or ATPase activity shown for each ligand concentration in *panels B–D* was determined from a time course performed as described under "Experimental Procedures."

by the QQG(p)TMVMPD peptide was achieved at a concentration of 40 ± 15 μM. Mutation of Arg^{734} to alanine abolished the ability of phosphothreonine to activate A-CAT-Δ809 (Fig. 6*C*) as did mutation of Asp^{762} to alanine (not shown). These results confirm that activation of A-CAT-Δ809 is the result of ligand binding to the P_i-pocket.

Phosphothreonine and the QQG(p)TMVMPD peptide also restored the ATPase activity of A-CAT-Δ809 (Fig. 6*D*). Both activators increased the ATPase activity of A-CAT-Δ809 to a level approaching 95% that of A-CAT. Half-maximal activation was achieved at QQG(p)TMVMPD and phosphothreonine concentrations of 120 ± 40 and 360 ± 40 μM, respectively. Taken together, the data show that phosphorylated ligands dramatically and specifically rescue the catalytic activity of A-CAT-Δ809.

Modeling of the C-tail at the P_i-pocket—Analytical ultracentrifugation studies show that A-CAT is a monomer in solu-

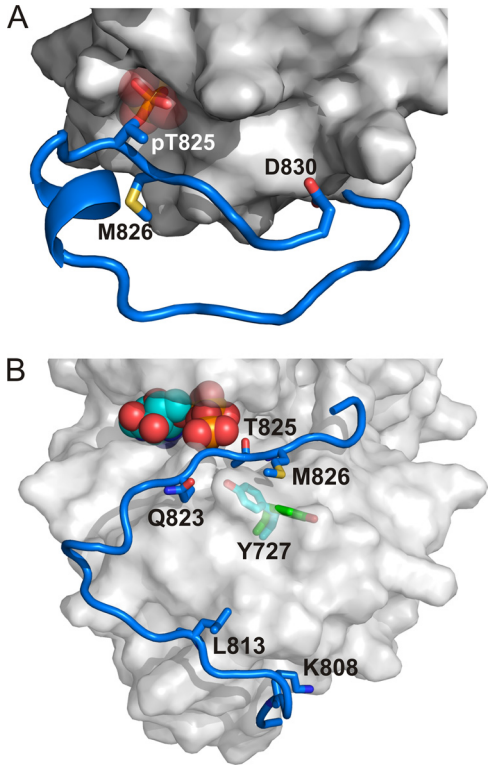

FIGURE 7. **Models of the C-tail bound to the P_i-pocket and active site.** The Rosetta FloppyTail and FlexPepDock protocols were used to model the C-tail (residues 806–830) using the procedure described under "Experimental Procedures." *A*, model of the C-tail with the phosphorylated Thr^{825} bound into the P_i-pocket. The C-tail is colored *blue*, key residues in the C-tail that interact with the α-kinase domain are shown in *stick* representation, and the original P_i in the crystal structure is represented as *transparent spheres*. The surface of A-CAT (PBD code 3LLA, chain B) is shown in *gray*. The model shows that the Thr^{825} phosphoryl group can act as an intramolecular ligand for the P_i-pocket. *B*, model of the C-tail with the unphosphorylated Thr^{825} at the active site. The C-tail is colored *blue*, residues in the C-tail that interact with the α-kinase domain are shown in *stick* representation, and ATP (from PBD code 3LMI) is shown as *spheres*. The surface of A-CAT is shown in *gray* and is transparent to illustrate the position of Tyr^{727} predicted by the model (*cyan sticks*) and in the crystal structure (*green sticks*). The model illustrates that it is feasible for Thr^{825} to be autophosphorylated via an intramolecular mechanism.

tion (23). To determine whether it is feasible for $Thr(P)^{825}$ to act as an intramolecular ligand for the P_i-pocket, residues 806–830 of the C-tail were modeled using the Rosetta FloppyTail and FlexPepDock protocols (40, 41). The only constraint on the model was that the Thr^{825} phosphoryl group was forced to adopt the same binding interactions as the P_i molecule in the crystal structure. The modeling process resulted in 5,500 independent models. The two top-scoring models converged on a single binding mode that allows $Thr(P)^{825}$ to dock into the P_i-pocket (Fig. 7*A* and supplemental Fig. S3). Reassuringly, the backbone and side chain conformations of residues 823–830 are nearly identical in both independent models. The model predicts that residues 806–817 form a random coil and make little or no contact with A-CAT, which is consistent with multiple sequence alignments that show this section of the C-tail to be poorly conserved (Fig. 2*A*). Residues 818–823 in the model form a short α-helix that, again, makes no contact with A-CAT. The conserved Gly^{824} allows the polypeptide chain to make a sharp turn that places the Thr^{825} phosphoryl group into the P_i-pocket in the same orientation as the P_i in the crystal structure. Residues on the C-terminal side of Thr^{825} take up an extended conformation and are involved in interactions with A-CAT. This stretch of sequence corresponds to the C-tail peptide (QQGTMVMPD) used in the A-CAT-Δ809 activation experiments described above. Most notably, Met^{826} makes hydrophobic contacts with Pro^{683} and Val^{799}.

Interestingly, the modeling studies predict that the side chain of Arg^{734} in the P_i-pocket can switch from the bent conformation present in the A-CAT crystal structure to a straight conformation (Fig. 5*C*). The conformational change moves the Arg^{734} guanidino group 3 to 6 Å away from the P_i pocket and thus disrupts the electrostatic interactions with the P_i molecule and Asp^{762}. The tendency of Arg^{734} to adopt the two orientations was evaluated by repacking the side chain conformations in the region of the P_i-pocket 200 times, both in the absence and presence of the C-tail. In the free state, 99.5% of the models had the side chain of Arg^{734} in the straight conformation, whereas when $Thr(P)^{825}$ is bound a significant fraction of the models (42.3%) had the Arg^{734} side chain in the bent conformation. These studies suggest that binding of a phosphorylated ligand induces a conformational change in Arg^{734} that promotes formation of a salt bridge with Asp^{762}.

Modeling of the C-tail in the Active Site—The same three-stage modeling protocol was carried out to examine whether it is feasible for Thr^{825} to interact in an intramolecular manner with the A-CAT active site. A soft constraint that required the Cβ atom of Thr^{825} to be within 3–6 Å of the Cβ atom of Asp^{756} (the presumed catalytic base) was applied in the initial low-resolution modeling using the FloppyTail protocol but was then removed in the subsequent high-resolution modeling steps. The modeling studies clearly indicate that the flexible C-tail allows Thr^{825} to access the active site (Fig. 7*B*). Although there was some convergence near the active site, the top-scoring models were not identical, indicating that the flexible C-tail is likely to be able to reach the catalytic site via an ensemble of conformations (supplemental Fig. S4). The top scoring model provides one possible snapshot of this ensemble and is stabilized by several favorable interactions, including a salt bridge between Lys^{808} and Glu^{746}, hydrophobic interactions between Leu^{813} and Thr^{793}, and a hydrogen bond between Gln^{822} and the main chain amide of Lys^{722} (Fig. 7*B*). In addition, the model predicts that the side chain of Tyr^{727} rotates from its position in the crystal structure toward the C-tail so that it can form a hydrogen bond with the side chain of Gln^{823} and participate in hydrophobic interactions with Met^{826}.

DISCUSSION

MHCK A is potently activated by autophosphorylation but the identity of the autophosphorylation sites and the mechanisms involved in the activation process have remained obscure. Previous studies have localized several MHCK-A autophosphorylation sites to a segment (amino acids 499–550) immediately N-terminal to the α-kinase domain (22). Studies on A-CAT, the isolated α-kinase domain of MHCK A, show that autophosphorylation of the N-terminal sites stimulates

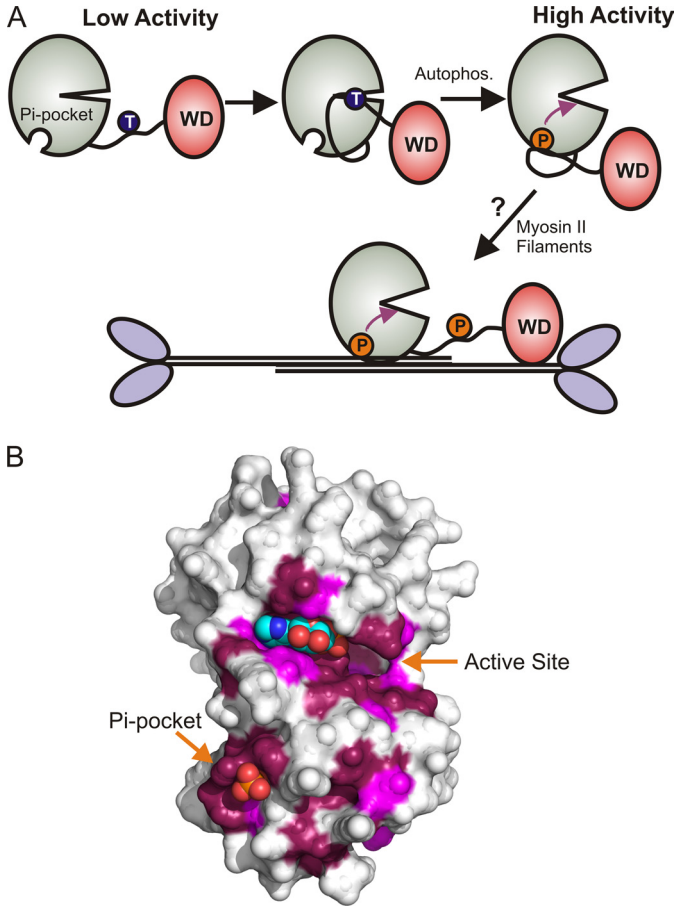

FIGURE 8. **A conserved activation mechanism for the MHCK/eEF2K family.** *A*, model for the activation of MHCK A. Only the α-kinase (*green*) and WD-repeat (*red*) domains of MHCK A are shown. MHCK A is in a low-activity state when the P_i-pocket in the α-kinase domain is empty. The intramolecular autophosphorylation of Thr^{825} in the disordered sequence connecting the α-kinase and WD-repeat domains provides a ligand for the P_i-pocket and induces a conformational change (*purple arrow*) that converts MHCK A to a high activity state. MHCK A is targeted to its physiological substrate, myosin II filaments, by the WD-repeat domain. It is speculated that the P_i-pocket could bind Thr(P) residues in the myosin II tail and promote the phosphorylation of adjacent threonine residues. *B*, the ConSurf server was used to map the conservation of amino acids, derived from a multiple sequence alignment of 20 MHCK/eEF2K homologues, onto the surface structure of A-CAT (PDB code 3LKM). Invariant residues (conservation score of 9) are colored *purple* and highly conserved residues (conservation score of 8) are colored *violet*. The P_i-pocket, the active site, and the N/D-loop represent the most highly conserved parts of the surface.

kinase activity by about 3-fold, yet deletion of the N-terminal segment has little effect on activity (22). These results were interpreted to indicate that the N-terminal segment may harbor an autoinhibitory sequence that is relieved by autophosphorylation. Here, we focus on the autophosphorylation of Thr^{825}, which is located in an unstructured sequence C-terminal to the α-kinase domain. Autophosphorylation of Thr^{825} is shown to be essential for the catalytic activity of A-CAT. We propose that $Thr(P)^{825}$ activates A-CAT by folding back onto the α-kinase domain, where it provides a ligand for an allosteric binding site, termed the P_i-pocket, that specifically recognizes phosphoamino acids (Fig. 8*A*).

Autophosphorylation of Thr^{825}—A-CAT purifies as a constitutively active monomer with full protein kinase activity (22, 23). Until the C-terminal truncation and mutagenesis studies described here, the key role played by autophosphorylation of Thr^{825} in promoting the activity of A-CAT had escaped detection. This can be attributed to the observation that Thr^{825} is constitutively phosphorylated in bacterially expressed A-CAT and that $Thr(P)^{825}$ is resistant to phosphatases, perhaps due to its ability to dock into the P_i-pocket. Thr^{825} does not have the features expected for a good A-CAT substrate. Most importantly, the $p + 1$, $p + 2$, $p + 3$, and $p + 4$ positions on the C-terminal side of Thr^{825} are occupied by hydrophobic residues instead of the lysine or arginine residues strongly preferred by A-CAT (21, 29). Indeed, we did not detect phosphorylation of the QQGTMVMPD peptide, which corresponds to the Thr^{825} phosphorylation site, when it was included in a kinase assay with A-CAT at a concentration of 0.5 mM (data not shown). The rapid autophosphorylation of Thr^{825} in the context of the C-tail is therefore likely to depend on a unimolecular autophosphorylation mechanism, in which Thr^{825} is presented to the active site at a very high effective concentration (C_{eff}) (Fig. 7*B*). A C_{eff} of 2.3 mM can be calculated for the tethered Thr^{825} based on the volume of a hemisphere with radius *r*, where *r* is the average (root mean square) length of the linker (~7 nm) connecting Thr^{825} to the α-kinase domain (43). The actual C_{eff} of Thr^{825} at the catalytic site might well be much greater than this as the result of favorable binding interactions between the C-tail and A-CAT (Fig. 7*B*). Although the top scoring model provides only one possible snapshot for how the C-tail may access the active site, it suggests some specific interactions that could be tested experimentally in future work. In particular, the hydrogen bond between the side chain of Gln^{823} in the $p - 2$ position and the side chain of Tyr^{727} provides a rationale for why A-CAT prefers to phosphorylate peptides with a hydrogen bond-forming residue (serine, threonine, or tyrosine) in the $p - 2$ position (29). However, the absence of basic residues means that the $p + 1$ to $p + 4$ positions in the C-tail will not bind to A-CAT in the same manner as good peptide substrates. Indeed, it can be speculated that the residues C-terminal to Thr^{825} may have evolved to favor binding at the P_i-pocket rather than at the active site.

The P_i-pocket Provides a Binding Site for $Thr(P)^{825}$ and Communicates with the Active Site—The results reported here show that loss of Thr^{825} severely inhibits both the kinase and ATPase activities of A-CAT. This rules out the possibility that $Thr(P)^{825}$ acts by facilitating the binding of peptide or protein substrates and instead points to a direct effect on the active site. The proposal that the P_i-pocket is the binding site for $Thr(P)^{825}$ is based on the following evidence: (i) the crystal structure of A-CAT identifies the P_i-pocket as a P_i-binding site; (ii) mutations that disrupted the P_i-pocket dramatically inhibited the activity of A-CAT; (iii) A-CAT-Δ809, which lacks the C-tail and Thr^{825}, could be specifically activated by phosphorylated ligands including P_i, phosphothreonine, and a phosphorylated peptide; (iv) activation by phosphorylated ligands was abolished by mutations (R734A, D762A) that disrupted the P_i-pocket; and (v) modeling studies demonstrated that it is feasible for $Thr(P)^{825}$ to provide an intramolecular ligand for the P_i-pocket.

Importantly, a molecular mechanism that allows the P_i-pocket to communicate directly with the active site is apparent from the crystal structure of A-CAT and gains support from the modeling studies (Fig. 5*C*). The mechanism hinges on a salt bridge that is formed between Arg^{734} in the P_i-pocket and Asp^{762} in the active site loop that harbors catalytic residues Asp^{756} and Asp^{766}. Asp^{766} accepts the γ-phosphate from ATP to form an aspartylphosphate intermediate and Asp^{756} is presumed to be the catalytic base in the phosphotransferase reaction (23, 44). By anchoring the catalytic loop, the salt bridge between Asp^{762} and Arg^{734} helps to fix the positions of Asp^{756} and Asp^{766} within the active site. The modeling studies indicate that the bent conformation of the Arg^{734} side chain that bridges the P_i molecule to Asp^{762} is not energetically favorable, especially when the P_i-pocket is empty. Thus, a plausible allosteric model can be proposed in which the binding of a phosphorylated ligand to the P_i-pocket stabilizes the bent conformation of the Arg^{734} side chain, which in turn promotes the electrostatic interaction with Asp^{762} and helps to properly align the Asp^{756}–Asp^{766} catalytic loop within the active site. It is interesting that interactions involving the Asp^{756}–Asp^{766} loop have also been implicated in the activation of TRPM7 by dimer assembly (45). The results suggest that regulatory mechanisms that stabilize what may be an inherently mobile Asp^{756}–Asp^{766} catalytic loop may provide a common pathway by which to activate the α-kinases.

In several experiments the kinase and ATPase activities of A-CAT were found to diverge. Phosphothreonine and the QQG(p)TMVMPD peptide restored about 60–65% of the kinase activity of A-CAT-Δ809 but close to 95% of the ATPase activity. Differential effects on the kinase and ATPase activities of A-CAT were also noted with the T825D, T825S, and Δ3 mutants (Figs. 2*B* and 4*C*). It can be speculated that the balance between the two enzymatic activities may depend on the active site conformation, which is influenced by the ligand for the P_i-pocket. Whether or not the ATPase (and ADPase) activities exhibited by A-CAT are physiologically relevant is currently not clear (23).

The identification of the P_i-pocket as a positive allosteric binding site provides a rationale for why A-CAT-Δ809 and A-CAT have virtually identical crystal structures. Both A-CAT and A-CAT-Δ809 were crystallized from buffers containing 0.2 M NaH_2PO_4 and in both crystal structures P_i occupies the P_i-pocket (23). It can be concluded that in the case of A-CAT, P_i in the crystallization buffer displaced $Thr(P)^{825}$ from the P_i-pocket, causing the C-tail to take up a disordered conformation that is not visible in the crystal structure. In the case of A-CAT-Δ809, P_i provided a ligand for the P_i-pocket in the absence of the C-tail and induced A-CAT-Δ809 to adopt the active conformation. This analysis highlights the need to identify crystallization conditions that lack P_i. In the absence of P_i, it may be possible to obtain a structure of the inactive state of A-CAT-Δ809 with an empty P_i-pocket and a structure of A-CAT in the autoactivated state with $Thr(P)^{825}$ docked into the P_i-pocket.

Substrate Specificity of the P_i-pocket—Glutamic acid and aspartic acid did not activate A-CAT-Δ809, although glutamic acid, and especially aspartic acid, supported a low level of catalytic activity when substituted for Thr^{835} in the C-tail. This suggests that the P_i-pocket exhibits a weak affinity for carboxyl groups. The primary interaction with the P_i-pocket is through the phosphoryl group. However, P_i was less effective than phosphothreonine in stimulating the activity of A-CAT-Δ809, indicating that the amino acid side chain plays some role in the binding interaction. The QQG(p)TMVMPD peptide activated A-CAT-Δ809 at a 3–5-fold lower concentration than phosphothreonine, which is consistent with the prediction from modeling studies that Met^{826} can act as a secondary recognition site to promote binding of the C-tail at the P_i-pocket (Fig. 7*A*). The importance of the potential secondary interactions in mediating the binding of Thr^{825} to the P_i-pocket can be tested experimentally in future work. The estimated binding affinity of the phosphorylated QQG(p)TMVMPD peptide for the P_i-pocket is in the range of 35–120 μM. This is well below the C_{eff} for the tethered Thr^{825} of 2.3 mM calculated above, and implies that autophosphorylation of Thr^{825} would be sufficient to saturate the P_i-pocket and fully switch on kinase activity.

A P_i-binding site has been identified in casein kinase I and glycogen synthase kinase 3β (46–48). In both cases, the P_i-binding site is located within the active site cleft and is responsible for the recognition of substrates that contain a phosphoamino acid. It is interesting to speculate that the P_i-pocket might act, along with the WD-repeat domain, to target MHCK A to bipolar myosin II filaments (Fig. 8*A*). Multiple threonine residues within each myosin II monomer need to be phosphorylated before the filament falls apart. Once one threonine residue in the filament is phosphorylated, it could act as a ligand for the P_i-pocket and enhance the rate of phosphorylation of nearby threonine residues (Fig. 8*A*). Such a mechanism could result in a more efficient disassembly of bipolar filaments and may provide an explanation for the ability of myosin II filaments to activate MHCK A (24). Negatively charged compounds, including DNA and vesicles composed of phosphatidylinositol, also activate MHCK A *in vitro* (26). The mechanism of activation is not known, but could involve the P_i-pocket. It will be important to establish whether the P_i-pocket is able to recognize phosphorylated lipids, nucleotides, and other phosphorylated molecules, or whether it is specific for phosphopeptides.

Conservation of the P_i-pocket in the MHCKs and eEF2Ks—Phylogenetic analysis demonstrates that the α-kinase domains of the *Dictyostelium* MHCKs and metazoan eEF2Ks group together to form one branch of the α-kinase family (12, 23). A multiple sequence alignment of the MHCKs and eEF2Ks shows that the residues that bind P_i (Lys^{684}, Arg^{734}, and Thr^{736}) and the aspartic acid that forms a salt bridge with Arg^{734} (Asp^{762}) are invariant (supplemental Fig. S5). The highly conserved nature of the P_i-pocket can be visualized by mapping residues conserved in the multiple sequence alignment onto the surface of A-CAT (Fig. 8*B*) (49). This result implies that an allosteric regulatory mechanism dependent on the binding of phosphorylated ligands may underlie the regulation of the entire MHCK/eEF2K family. Although the C-tail sequences of the MHCK/eEF2K family members are divergent, a threonine residue followed by a hydrophobic residue is

always present (supplemental Fig. S5). The conserved nature of the hydrophobic residue in the $p + 1$ position is consistent with the observation that its predicted binding partner, Pro^{683}, is an invariant residue in the MHCK/eEF2K family (supplemental Fig. S5). eEF2K rapidly autophosphorylates multiple serine and threonine residues via an intramolecular mechanism but the sites have not been mapped (50). Several residues in the C-tail of eEF2K are targets for exogenous protein kinases and their phosphorylation can either inhibit or activate kinase activity (20). Further studies will be required to determine whether any of the C-tail phosphorylation sites regulate eEF2K by acting as a ligand for the P_i-pocket.

In summary, we have demonstrated that the α-kinase domain of MHCK A contains a previously undetected allosteric binding site for phosphorylated peptides. The allosteric binding site provides a mechanism to switch on the activity of MHCK A in response to autophosphorylation and is likely to play a central role in regulating the cellular activities of MHCK A and its close homologues, including eEF2K.

Acknowledgments—We thank David McLeod of the Protein Function Discovery Facility, Queen's University for carrying out mass spectrometry experiments. Portions of this research were carried out at the Cornell High Energy Synchrotron Source.

REFERENCES

1. Côte, G. P., and Bukiejko, U. (1987) *J. Biol. Chem.* **262,** 1065–1072
2. De La Roche, M. A., Smith, J. L., Betapudi, V., Egelhoff, T. T., and Côté, G. P. (2002) *J. Muscle Res. Cell Motil.* **23,** 703–718
3. Vaillancourt, J. P., Lyons, C., and Côté, G. P. (1988) *J. Biol. Chem.* **263,** 10082–10087
4. Lück-Vielmetter, D., Schleicher, M., Grabatin, B., Wippler, J., and Gerisch, G. (1990) *FEBS Lett.* **269,** 239–243
5. Kolman, M. F., Futey, L. M., and Egelhoff, T. T. (1996) *J. Cell Biol.* **132,** 101–109
6. Egelhoff, T. T., Lee, R. J., and Spudich, J. A. (1993) *Cell* **75,** 363–371
7. Futey, L. M., Medley, Q. G., Côté, G. P., and Egelhoff, T. T. (1995) *J. Biol. Chem.* **270,** 523–529
8. Steimle, P. A., Licate, L., Côté, G. P., and Egelhoff, T. T. (2002) *FEBS Lett.* **516,** 58–62
9. Russ, M., Croft, D., Ali, O., Martinez, R., and Steimle, P. A. (2006) *Biochem. J.* **395,** 373–383
10. Kolman, M. F., and Egelhoff, T. T. (1997) *J. Biol. Chem.* **272,** 16904–16910
11. Steimle, P. A., Naismith, T., Licate, L., and Egelhoff, T. T. (2001) *J. Biol. Chem.* **276,** 6853–6860
12. Middelbeek, J., Clark, K., Venselaar, H., Huynen, M. A., and Van Leeuwen, F. N. (2010) *Cell Mol. Life Sci.* **67,** 875–890
13. Yumura, S., Yoshida, M., Betapudi, V., Licate, L. S., Iwadate, Y., Nagasaki, A., Uyeda, T. Q., and Egelhoff, T. T. (2005) *Mol. Biol. Cell* **16,** 4256–4266
14. Nagasaki, A., Itoh, G., Yumura, S., and Uyeda, T. Q. (2002) *Mol. Biol. Cell* **13,** 4333–4342
15. Liang, W., Licate, L., Warrick, H., Spudich, J., and Egelhoff, T. (2002) *BMC Cell Biol.* **3,** 19
16. Betapudi, V., Mason, C., Licate, L., and Egelhoff, T. T. (2005) *Mol. Biol. Cell* **16,** 2248–2262
17. Betapudi, V., and Egelhoff, T. T. (2009) *Traffic* **10,** 1773–1784
18. Clark, K., Langeslag, M., van Leeuwen, B., Ran, L., Ryazanov, A. G., Figdor, C. G., Moolenaar, W. H., Jalink, K., and van Leeuwen, F. N. (2006) *EMBO J.* **25,** 290–301
19. Clark, K., Middelbeek, J., Lasonder, E., Dulyaninova, N. G., Morrice, N. A., Ryazanov, A. G., Bresnick, A. R., Figdor, C. G., and Van Leeuwen, F. N. (2008) *J. Mol. Biol.* **378,** 790–803
20. Proud, C. G. (2007) *Biochem. J.* **403,** 217–234
21. Luo, X., Crawley, S. W., Steimle, P. A., Egelhoff, T. T., and Cote, G. P. (2001) *J. Biol. Chem.* **276,** 17836–17843
22. Côté, G. P., Luo, X., Murphy, M. B., and Egelhoff, T. T. (1997) *J. Biol. Chem.* **272,** 6846–6849
23. Ye, Q., Crawley, S. W., Yang, Y., Côté, G. P., and Jia, Z. (2010) *Sci. Signal.* **3,** ra17
24. Medley, Q. G., Gariépy, J., and Côté, G. P. (1990) *Biochemistry* **29,** 8992–8997
25. Egelhoff, T. T., Croft, D., and Steimle, P. A. (2005) *J. Biol. Chem.* **280,** 2879–2887
26. Medley, Q. G., Bagshaw, W. L., Truong, T., and Côté, G. P. (1992) *Biochim. Biophys. Acta* **1175,** 7–12
27. Sambrook, J., Fritsch, E. F., and Maniatis, T. (1989) *Molecular Cloning: A Laboratory Manual*, 2nd Ed., Cold Spring Harbor Laboratory, Cold Spring Harbor, NY
28. Levi, S., Polyakov, M., and Egelhoff, T. T. (2000) *Plasmid* **44,** 231–238
29. Crawley, S. W., and Côté, G. P. (2008) *Biochim. Biophys. Acta* **1784,** 908–915
30. Hadwiger, J. A., and Firtel, R. A. (1992) *Genes Dev.* **6,** 38–49
31. Sussman, M. (1987) *Methods Cell Biol.* **28,** 9–29
32. Knecht, D. A., and Shelden, E. (1995) *Dev. Biol.* **170,** 434–444
33. Crawley, S. W., de la Roche, M. A., Lee, S. F., Li, Z., Chitayat, S., Smith, S. P., and Côté, G. P. (2006) *J. Biol. Chem.* **281,** 6307–6315
34. Pollard, T. D., and Korn, E. D. (1973) *J. Biol. Chem.* **248,** 4682–4690
35. Casnellie, J. E. (1991) *Methods Enzymol.* **200,** 115–120
36. Otwinowski, Z., and Minor, W. (1997) in *Methods in Enzymology* (Carter, C., and Sweet, R., eds) Vol. 276, pp. 307–326, Academic Press, New York
37. McCoy, A. J., Grosse-Kunstleve, R. W., Storoni, L. C., and Read, R. J. (2005) *Acta Crystallogr. D Biol. Crystallogr.* **61,** 458–464
38. Brünger, A. T., Adams, P. D., Clore, G. M., DeLano, W. L., Gros, P., Grosse-Kunstleve, R. W., Jiang, J. S., Kuszewski, J., Nilges, M., Pannu, N. S., Read, R. J., Rice, L. M., Simonson, T., and Warren, G. L. (1998) *Acta Crystallogr. D Biol. Crystallogr.* **54,** 905–921
39. Murshudov, G. N., Vagin, A. A., Lebedev, A., Wilson, K. S., and Dodson, E. J. (1999) *Acta Crystallogr. D Biol. Crystallogr.* **55,** 247–255
40. Kleiger, G., Saha, A., Lewis, S., Kuhlman, B., and Deshaies, R. J. (2009) *Cell* **139,** 957–968
41. Raveh, B., London, N., and Schueler-Furman, O. (2010) *Proteins* **78,** 2029–2040
42. Wang, C., Bradley, P., and Baker, D. (2007) *J. Mol. Biol.* **373,** 503–519
43. Kramer, R. H., and Karpen, J. W. (1998) *Nature* **395,** 710–713
44. Yamaguchi, H., Matsushita, M., Nairn, A. C., and Kuriyan, J. (2001) *Mol. Cell* **7,** 1047–1057
45. Crawley, S. W., and Côté, G. P. (2009) *Biochem. J.* **420,** 115–122
46. Xu, R. M., Carmel, G., Sweet, R. M., Kuret, J., and Cheng, X. (1995) *EMBO J.* **14,** 1015–1023
47. Dajani, R., Fraser, E., Roe, S. M., Young, N., Good, V., Dale, T. C., and Pearl, L. H. (2001) *Cell* **105,** 721–732
48. Longenecker, K. L., Roach, P. J., and Hurley, T. D. (1996) *J. Mol. Biol.* **257,** 618–631
49. Glaser, F., Pupko, T., Paz, I., Bell, R. E., Bechor-Shental, D., Martz, E., and Ben-Tal, N. (2003) *Bioinformatics* **19,** 163–164
50. Redpath, N. T., and Proud, C. G. (1993) *Eur. J. Biochem.* **212,** 511–520